

Investigation of Time-Frequency Feature Combinations with Histogram Layer Time Delay Neural Networks

Amirmohammad Mohammadi, Irené Masabarakiza, Ethan Barnes, Davelle Carreiro, Alexandra Van Dine, and Joshua Peebles, *Member, IEEE*

Abstract—While deep learning has reduced the prevalence of manual feature extraction, transformation of data via feature engineering remains essential for improving model performance, particularly for underwater acoustic signals. The methods by which audio signals are converted into time-frequency representations and the subsequent handling of these spectrograms can significantly impact performance. This work demonstrates the performance impact of using different combinations of time-frequency features in a histogram layer time delay neural network. An optimal set of features is identified with results indicating that specific feature combinations outperform single data features.

Index Terms—deep learning, underwater acoustic classification, histogram layers, feature engineering

I. INTRODUCTION

DRIVEN by an ability to effectively process large volumes of data, deep learning (DL) has been successfully used for acoustic classification tasks [1], [2]. One application of sound classification is Underwater Acoustic Target Recognition (UATR), where acoustic signals are used to classify underwater objects. This technology has various applications in marine environments such as biological pattern of life determination, search and rescue, seabed mapping, and shipping traffic monitoring [3], [4]. DL methods are being widely developed due to their effective ability in processing time-frequency features generated from raw input signals and performing end-to-end tasks such as classification for underwater acoustic signals [5]–[7]. While DL can automatically extract and learn

features, the transformation and manipulation of audio signals is an important step of feature engineering [8].

Generally, time-domain sound signals are first converted into time-frequency representations, known as spectrograms, before being processed by artificial neural networks [9]. This is useful because spectral representations contain unique acoustic signatures of underwater objects, allowing models like convolutional neural networks (CNNs) to learn from these patterns. Success with this method has been demonstrated in image analysis tasks [10].

Images can be decomposed into statistical and structural texture features [11]–[13]. Spectrograms can also be represented through these two texture types. Statistical texture features provide information about the acoustic texture [14], using statistical measures that usually capture the distribution of textures. Structural texture features, on the other hand, are the spatial patterns of textures [15]. Models like CNNs and time delay neural networks (TDNNs), are very effective at capturing spatial and temporal arrangements, or structural textures in imagery such as spectrograms [13]. However, these models may not fully take into account the statistical features within spectrograms.

Histogram layers are designed to model the distribution of feature values within local regions of images [15]. The motivation is that histogram layers directly model statistical features by characterizing spatial distributions of features as opposed to other deep learning approaches such as CNNs. The integration of these layers into TDNNs, referred to as Histogram Layer Time Delay Neural Network (HLTDNN), [16] improved classification performance for UATR. This addition improved capture of statistical context, thereby providing a more accurate representation of the feature distributions across local spatial regions [15]. Prior work [16] on the HLTDNN used single spectrogram data inputs for classification.

The representation of audio signals is a difficult problem yet crucial to the success of machine learning algorithms [17]. Related work [18] has demonstrated that combining three types of spectrograms, mel-frequency spectrograms, gammatone-frequency spectrograms (Cochleagrams), and continuous wavelet transforms (CWT), can improve the detection of speech deficits in cochlear implant users. The task of acoustic feature engineering, particularly for underwater environments, still remains challenging [19]. While a prior study showed feature fusion to be effective in improving UATR performance [20], it focused on a smaller UATR dataset, ShipsEar

DISTRIBUTION STATEMENT A. Approved for public release. Distribution is unlimited. This material is based upon work supported by the Under Secretary of Defense for Research and Engineering under Air Force Contract No. FA8702-15-D-0001. Any opinions, findings, conclusions or recommendations expressed in this material are those of the author(s) and do not necessarily reflect the views of the Under Secretary of Defense for Research and Engineering. © 2024 Massachusetts Institute of Technology. Delivered to the U.S. Government with Unlimited Rights, as defined in DFARS Part 252.227-7013 or 7014 (Feb 2014). Notwithstanding any copyright notice, U.S. Government rights in this work are defined by DFARS 252.227-7013 or DFARS 252.227-7014 as detailed above. Use of this work other than as specifically authorized by the U.S. Government may violate any copyrights that exist in this work. Code is publicly available at https://github.com/Advanced-Vision-and-Learning-Lab/HLTDNN_Feature_Combination.

Amirmohammad Mohammadi, Irené Masabarakiza, Ethan Barnes, and Joshua Peebles are with the Department of Electrical and Computer Engineering, Texas A&M University, College Station, TX, USA (e-mail: amir.m@tamu.edu; imasabo2k18@tamu.edu; ecbarnes@tamu.edu; jpeeples@tamu.edu).

Davelle Carreiro and Alexandra Van Dine are with the Massachusetts Institute of Technology Lincoln Laboratory, Lexington, MA, USA (e-mail: davelle.carreiro@ll.mit.edu; alexandra.vandine@ll.mit.edu).

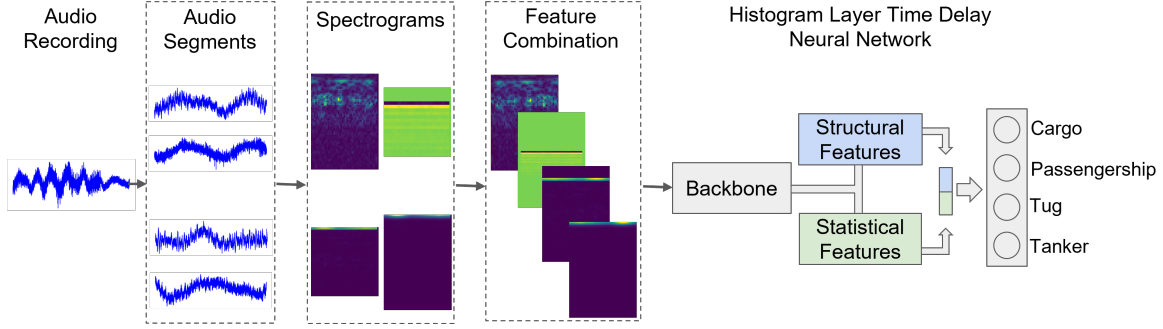


Fig. 1: Overall workflow of this work. The audio segments are first partitioned into individual segments. Each audio segment is then used to compute an individual feature of varying time and frequency resolutions. We introduce an adaptive padding layer to make each spectrogram the same size. The features are then concatenated along the channel dimension and processed by the HLTDNN model for classification.

[21]. A related effort [22] used a larger dataset, DeepShip [23], to show that feature fusion could improve performance, but did not investigate the impact of feature selection for three spectrogram features used. Additionally, spectrograms for the inputs are restricted to be the same size and cannot use different hyperparameters (*e.g.*, window length, hop length) for each spectrogram which may unintentionally restrict the unique information captured by each feature.

We leverage the HLTDNN in our work, and focus on extending the application of spectrogram techniques by investigating various combinations of acoustic data features to find an optimal set of features which yields improved classification performance. This approach is driven by the hypothesis that a combination of acoustic data features could provide a richer representation of the input signals [24]. To our knowledge, this is the first investigation of feature combinations for the DeepShip dataset using HLTDNNs.

II. METHOD

A. Review of the HLTDNN architecture and the histogram layer operation

The HLTDNN's [16] backbone consists of multiple convolution layers that have the rectified linear unit (ReLU) activation function, followed by max pooling layers. The histogram layer is positioned in parallel to another convolutional block. The input into both the histogram layer and convolutional blocks are from the the fourth convolutional block. The histogram layer captures statistical texture information while the convolutional block focuses on structural texture information. The statistical and structural features are concatenated together and passed into the output classification layer [15], [16].

Let $\mathbf{X} \in \mathbb{R}^{M \times N \times D}$ be the input to a histogram layer, where M, N are spatial dimensions and D is feature dimensionality. Applying a histogram layer with B bins yields output $\mathbf{Y} \in \mathbb{R}^{R \times C \times B \times D}$, where R, C are output spatial dimensions determined by kernel size $S \times T$:

$$Y_{rcbd} = \frac{1}{ST} \sum_{s=1}^S \sum_{t=1}^T e^{-\gamma_{bd}^2 (x_{r+s, c+t, d} - \mu_{bd})^2} \quad (1)$$

Here, μ_{bd} and γ_{bd} are learnable bin centers and widths. The layer processes each input feature dimension, producing BD histogram feature maps. It uses radial basis functions to determine feature contributions to bins, capturing feature value distributions and adding statistical context to the model.

B. Feature combination implementation

We propose merging different spectrogram features to potentially improve the representational power of the input data passed into the model. Given a total of \mathcal{M} unique time-frequency features, the total number of unique combinations, \mathcal{N} , can be computed as $\mathcal{N} = 2^{\mathcal{M}} - 1$. For our work, six different time-frequency features are combined to generate 63 distinct combinations ($2^6 - 1$). To prepare these combination of features for input into the model, an adaptive zero padding layer is incorporated into the spectrograms. During adaptive padding, since features do not share the same height and width dimensions, they are resized to a common dimension, as to be combined without losing their time-frequency resolution by calculating the required padding for each side of a feature map to match the largest height and width among all features. Padding is applied symmetrically to maintain the feature's original structure and position within its new dimensions. Once all features are resized to a uniform dimension, they are combined by concatenating the feature maps along the channel dimension. The overall workflow is shown in Fig. 1.

III. EXPERIMENTAL SETUP

In this work, the DeepShip sonar dataset is used [23]. This dataset has a collection of real-world sonar recordings with 265 different ships across four classes (tanker, tug, passengership, and cargo), compiled from 47 hours and 4 minutes of recordings. Recordings are captured under various sea states and noise levels. Audio signals are resampled to a frequency of 16 kHz and then segmented into intervals of three seconds. Next, six time-frequency based features are extracted: mel-frequency spectrogram (MS), mel-frequency cepstral coefficients (MFCCs), short-time fourier transform (STFT), gammatone-frequency cepstral coefficients (GFCC), constant-q transform (CQT), and variable-q transform (VQT).

TABLE I: Overall performance metrics including the Matthews Correlation Coefficient (MCC) for the top five combinations and the best single feature. The results shown are based on the average value with $\pm 1\sigma$ across the three experimental runs of random initialization. For brevity, we show the top five feature combinations. The full set of results can be found in the code repository.

Features	Accuracy (%)	Precision (%)	Recall (%)	F1 score (%)	MCC
VQT, MFCC, STFT, GFCC	66.17 \pm 1.10	67.17 \pm 1.53	66.17 \pm 1.10	65.95 \pm 1.17	0.548 \pm 0.015
MS, CQT, MFCC, STFT	65.69 \pm 1.68	66.01 \pm 2.69	65.69 \pm 1.68	65.00 \pm 2.04	0.544 \pm 0.023
MFCC, STFT, GFCC	65.55 \pm 1.02	66.32 \pm 1.92	65.55 \pm 1.02	64.85 \pm 1.16	0.543 \pm 0.016
CQT, MFCC, STFT	65.49 \pm 0.65	66.47 \pm 0.62	65.49 \pm 0.65	64.78 \pm 1.07	0.547 \pm 0.006
MS, MFCC, STFT, GFCC	64.89 \pm 1.12	66.36 \pm 1.08	64.89 \pm 1.12	63.91 \pm 1.19	0.540 \pm 0.012
MFCC	59.34 \pm 3.16	60.46 \pm 1.83	59.34 \pm 3.16	58.37 \pm 3.88	0.461 \pm 0.036

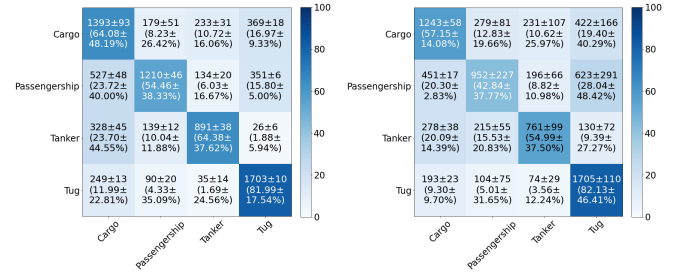
Studies have demonstrated the effectiveness of these features in classifying underwater acoustic signals [16], [23], [25]. For the extraction process, the window and hop length are set at 250 ms and 64 ms, respectively. Specifically, MS uses 44 Mel filter banks. In the case of MFCCs, there are 16 mel-frequency cepstral coefficients. Meanwhile, STFT has 48 frequency bins. For the GFCC, CQT, and VQT features, there are 64 frequency bins.

The dataset was partitioned into training, validation, and test sets with respective ratios of 70%, 15%, and 15% based on [16]. A total of 56,468 segments were generated, distributed as 38,523 for training, 9,065 for validation, and 8,880 for testing. To prevent data leakage, segments derived from a single recording were exclusively allocated to the same partition. This ensures if a recording is chosen for training, all its segments are also chosen solely for training purposes. The HLTDNN model was evaluated with each combination of features across three runs of random initialization. The configuration for the experimental parameters was as follows: Adagrad optimizer with a learning rate of 0.001 and training batch size of 128. A dropout rate of 0.5 was applied preceding the output classification layer to mitigate overfitting. Additionally, early stopping was implemented to stop training if no improvement in validation loss is observed after 15 epochs. The maximum epoch number was set to 150. Following [16], the number of bins was set to 16 for the HLTDNN model. Experiments were completed on an A100 GPU.

IV. RESULTS AND DISCUSSION

The top five feature combinations and best single feature (MFCC) performance metrics are reported in Table I. In evaluating the performance of the model across various feature combinations, it was observed that the combination of VQT, MFCC, STFT, and GFCC features resulted in the highest classification performance across multiple metrics. This new combination achieved an accuracy of $66.17 \pm 1.10\%$ and outperformed the highest accuracy of the single input feature case, $59.34 \pm 3.16\%$, using MFCC alone. Therefore, an increase of 6.83% in accuracy is achieved. This result shows the synergistic effect of combining acoustic features for UATR.

The best-performing feature combination was then further analyzed using a confusion matrix and t-SNE visualization to investigate classification details and feature space distribution, respectively. These visuals show the differentiation between classes. The confusion matrix and the t-SNE for both the best feature combination and the best single feature are shown in



(a) Best: $66.17 \pm 1.10\%$ (b) MFCC: $59.34 \pm 3.16\%$

Fig. 2: Comparison of confusion matrix results for the best combination of features and MFCC alone.

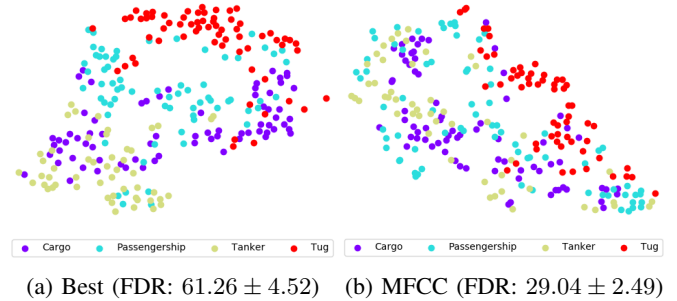


Fig. 3: t-SNE results for the best feature combination and MFCC. Colors show the four classes of ships. The average log Fisher Discriminant Ratio (FDR) ($\pm 1\sigma$) is also shown. Higher scores show more compact and better separated classes. The best random seed is used for each feature.

Figs. 2 and 3, respectively. In the confusion matrices, it is noted that the combination of features led to reduced variability in model prediction. The best feature combination resulted in reduced standard deviation in correct prediction for three of the four vessel types (passengership, tanker, tug). It is also noted that the best features led to improved performance for cargo, passengership and tanker with comparable performance seen for the tug class when compared to MFCC alone.

The log Fisher's Discriminant Ratio (FDR) was computed as a measure to evaluate the separability of the features by considering the distance between class means, normalized by the variance within each class. For the best feature combination, higher FDR scores and the t-SNE visualizations in Fig. 3 show strong performance compared to the single feature

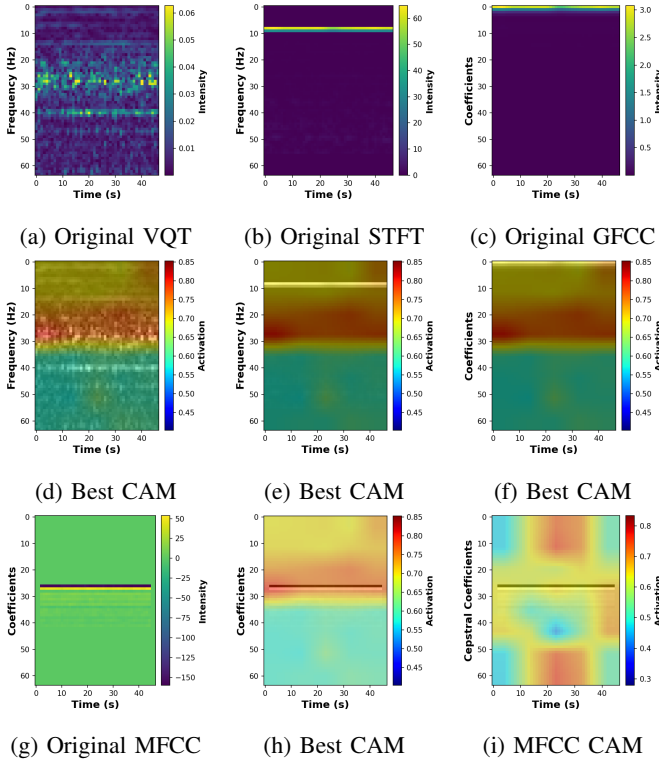


Fig. 4: Class Activation Maps (CAM) using the best feature combination and MFCC alone for the Cargo class. The third row compares the CAM overlay on the MFCC for both of the models.

where there is more overlap between classes. Specifically, passengership data points are more compact and centered for the best combination of features while tug data points are more separated. The best random seed initialization (*i.e.*, experimental run with the best performance metrics) was used for each t-SNE visualization to compare the best feature combination and a single feature (MFCC). Along with fixing the random seed, the number of features from the penultimate layer is the same for the feature combination and MFCC (\mathbb{R}^{512}) since the HLTDDN model uses an adaptive average pooling layer in the base architecture [16].

The reason that the model using combined features is performing better can be explained by the unique characterizations of the acoustic signal that each spectrogram contains. The repeated appearance of MFCC and STFT across the top-performing combinations shows that they are capturing more impactful signal characteristics. Each feature is sensitive to different aspects of the sound signal and for each type of ship, specific patterns can be found in the spectrograms due to the unique properties of their acoustic emissions. For example, the low-frequency content can be dominated by a propeller signature [23]. MFCC have proven effective in representing these sound signals, using a mel scale that approximates the human auditory system’s response [23], [26], [27]. Similarly, GFCCs are computed with a gammatone filter bank effective for the analysis of low-frequency sounds [28]. VQT provides improved frequency resolution at low frequencies and better

time resolution at high frequencies [29]–[31]. STFT is noted for its effectiveness in analyzing narrowband signals by producing a consistent set of local spectra across time intervals [32], [33]. The reason MS and CQT are not present in the top feature combination might be due to their potential overlap in contributions with other features. Specifically, VQT somewhat covers CQT, and the information captured by MS might be sufficiently represented by the combination of MFCC, GFCC, and STFT.

Explainable artificial intelligence (XAI), specifically the FullGrad Class Activation Mapping (FullCAM) method [34], is used to analyze the model’s decision-making process as shown in Fig. 4. For illustration, this method was applied to analyze the cargo class. By overlaying CAM on spectrograms of the best feature combinations as well as MFCC alone, the model’s focus areas for classification decisions can be seen. This specific sample was correctly classified by the best feature combination model but was misclassified by the MFCC model. Colors indicate the importance a model placed on a particular component of the data feature. The CAM output difference between the best feature combination and MFCC alone shows that the model using the combined features is more focused on specific frequency bands. MFCC alone is focusing on a different range of frequencies and potentially cannot achieve the same discriminative ability. FullCAM shows how important different parts of the data are by looking at the gradients of the biases from all layers of the network, unlike other methods that focus on certain layer(s) in the network. This helps provide insight into which specific frequencies appear more important in the input spectrogram for classification as the network is focusing on these regions of the time-frequency feature throughout the model.

V. CONCLUSION

Our work shows the importance of feature selection to improve the performance of the HLTDDN model, particularly in the context of acoustic signal processing. The pipeline was adapted to process acoustic data feature combinations to better capture representations of the acoustic signals. It is concluded that the combination of VQT, MFCC, STFT, and GFCC outperforms other combinations especially when compared to the best single feature, MFCC. Future work includes investigating the integration of learnable feature representations, potentially through end-to-end DL models that can automatically optimize feature combinations. Additionally, while an exhaustive search of feature combinations can find the optimal solution [35], this approach is not computationally efficient [35], [36]. Other approaches such as filter-based feature selection techniques can improve the computational cost of “pre-screening” features instead of generating, training, and evaluating a model for each feature [35], [37].

REFERENCES

- [1] Y. Qu, X. Li, Z. Qin, and Q. Lu, “Acoustic scene classification based on three-dimensional multi-channel feature-correlated deep learning networks,” *Scientific Reports*, vol. 12, no. 1, p. 13730, 2022.
- [2] W. Mu, B. Yin, X. Huang, J. Xu, and Z. Du, “Environmental sound classification using temporal-frequency attention based convolutional neural network,” *Scientific Reports*, vol. 11, no. 1, p. 21552, 2021.

- [3] A. Testolin, D. Kipnis, and R. Diamant, "Detecting submerged objects using active acoustics and deep neural networks: A test case for pelagic fish," *IEEE Transactions on Mobile Computing*, vol. 21, no. 8, pp. 2776–2788, 2020.
- [4] B. Beckler, A. Pfau, M. Orescanin, S. Atchley, N. Villemez, J. E. Joseph, C. W. Miller, and T. Margolina, "Multilabel classification of heterogeneous underwater soundscapes with bayesian deep learning," *IEEE Journal of Oceanic Engineering*, vol. 47, no. 4, pp. 1143–1154, 2022.
- [5] S. Feng and X. Zhu, "A transformer-based deep learning network for underwater acoustic target recognition," *IEEE Geoscience and Remote Sensing Letters*, vol. 19, pp. 1–5, 2022.
- [6] S. Tian, D. Chen, H. Wang, and J. Liu, "Deep convolution stack for waveform in underwater acoustic target recognition," *Scientific reports*, vol. 11, no. 1, p. 9614, 2021.
- [7] B. Wang, W. Zhang, Y. Zhu, C. Wu, and S. Zhang, "An underwater acoustic target recognition method based on amnet," *IEEE Geoscience and Remote Sensing Letters*, vol. 20, pp. 1–5, 2023.
- [8] H. Purwins, B. Li, T. Virtanen, J. Schlüter, S.-Y. Chang, and T. Sainath, "Deep learning for audio signal processing," *IEEE Journal of Selected Topics in Signal Processing*, vol. 13, no. 2, pp. 206–219, 2019.
- [9] K. Zaman, M. Sah, C. Direkoglu, and M. Unoki, "A survey of audio classification using deep learning," *IEEE Access*, vol. 11, pp. 106 620–106 649, 2023.
- [10] F. Liu, T. Shen, Z. Luo, D. Zhao, and S. Guo, "Underwater target recognition using convolutional recurrent neural networks with 3-d mel-spectrogram and data augmentation," *Applied Acoustics*, vol. 178, p. 107989, 2021.
- [11] A. Ramola, A. K. Shakya, and D. Van Pham, "Study of statistical methods for texture analysis and their modern evolutions," *Engineering Reports*, vol. 2, no. 4, p. e12149, 2020.
- [12] T. Özseven, "Investigation of the effect of spectrogram images and different texture analysis methods on speech emotion recognition," *Applied Acoustics*, vol. 142, pp. 70–77, 2018.
- [13] D. Ji, H. Wang, M. Tao, J. Huang, X.-S. Hua, and H. Lu, "Structural and statistical texture knowledge distillation for semantic segmentation," in *Proceedings of the IEEE/CVF Conference on Computer Vision and Pattern Recognition*, 2022, pp. 16 876–16 885.
- [14] M. Trevorrow, "Examination of statistics and modulation of underwater acoustic ship signatures," 2021.
- [15] J. Peeples, W. Xu, and A. Zare, "Histogram layers for texture analysis," *IEEE Transactions on Artificial Intelligence*, vol. 3, no. 4, pp. 541–552, 2021.
- [16] J. Ritu, E. Barnes, R. Martell, A. Van Dine, and J. Peeples, "Histogram layer time delay neural networks for passive sonar classification," in *2023 IEEE Workshop on Applications of Signal Processing to Audio and Acoustics (WASPAA)*. IEEE, 2023, pp. 1–5.
- [17] G. Sharma, K. Umapathy, and S. Krishnan, "Trends in audio signal feature extraction methods," *Applied Acoustics*, vol. 158, p. 107020, 2020.
- [18] T. Arias-Vergara, P. Klumpp, J. C. Vazquez-Correa, E. Nöth, J. R. Orozco-Arroyave, and M. Schuster, "Multi-channel spectrograms for speech processing applications using deep learning methods," *Pattern Analysis and Applications*, vol. 24, pp. 423–431, 2021.
- [19] M. A. Aslam, L. Zhang, X. Liu, M. Irfan, Y. Xu, N. Li, P. Zhang, Z. Jiangbin, and L. Yaan, "Underwater sound classification using learning based methods: A review," *Expert Systems with Applications*, vol. 255, p. 124498, 2024.
- [20] X. Ke, F. Yuan, and E. Cheng, "Integrated optimization of underwater acoustic ship-radiated noise recognition based on two-dimensional feature fusion," *Applied Acoustics*, vol. 159, p. 107057, 2020.
- [21] D. Santos-Domínguez, S. Torres-Guijarro, A. Cardenal-López, and A. Pena-Gimenez, "Shipsear: An underwater vessel noise database," *Applied Acoustics*, vol. 113, pp. 64–69, 2016.
- [22] W. Zhang, B. Lin, Y. Yan, A. Zhou, Y. Ye, and X. Zhu, "Multi-features fusion for underwater acoustic target recognition based on convolution recurrent neural networks," in *2022 8th International Conference on Big Data and Information Analytics (BigDIA)*. IEEE, 2022, pp. 342–346.
- [23] M. Irfan, Z. Jiangbin, S. Ali, M. Iqbal, Z. Masood, and U. Hamid, "Deepship: An underwater acoustic benchmark dataset and a separable convolution based autoencoder for classification," *Expert Systems with Applications*, vol. 183, p. 115270, 2021.
- [24] Z. Chi, Y. Li, and C. Chen, "Deep convolutional neural network combined with concatenated spectrogram for environmental sound classification," in *2019 IEEE 7th International Conference on Computer Science and Network Technology (ICCSNT)*, 2019.
- [25] T. Guo, Y. Song, Z. Kong, E. Lim, M. López-Benítez, F. Ma, and L. Yu, "Underwater target detection and localization with feature map and cnn-based classification," in *2022 4th International Conference on Advances in Computer Technology, Information Science and Communications (CTISC)*. IEEE, 2022, pp. 1–8.
- [26] T. Guo, Y. Song, Z. Kong, E. Lim, M. López-Benítez, F. Ma, and L. Yu, "Underwater target detection and localization with feature map and cnn-based classification," in *2022 4th International Conference on Advances in Computer Technology, Information Science and Communications (CTISC)*, 2022, pp. 1–8.
- [27] Z. K. Abdul and A. K. Al-Talabani, "Mel frequency cepstral coefficient and its applications: A review," *IEEE Access*, vol. 10, pp. 122 136–122 158, 2022.
- [28] Z. Lian, K. Xu, J. Wan, and G. Li, "Underwater acoustic target classification based on modified gfcc features," in *2017 IEEE 2nd Advanced Information Technology, Electronic and Automation Control Conference (IAEAC)*, 2017, pp. 258–262.
- [29] C. Schörkhuber and A. Klapuri, "Constant-q transform toolbox for music processing," *Proc. 7th Sound and Music Computing Conf.*, 01 2010.
- [30] X. Cao, R. Togneri, X. Zhang, and Y. Yu, "Convolutional neural network with second-order pooling for underwater target classification," *IEEE Sensors Journal*, vol. 19, no. 8, pp. 3058–3066, 2019.
- [31] C. Schörkhuber, A. Klapuri, N. Holighaus, and M. Doerfler, "A matlab toolbox for efficient perfect reconstruction time-frequency transforms with log-frequency resolution," 01 2014.
- [32] H. Jia, X. Li, and X. Meng, "Rigid and elastic acoustic scattering signal separation for underwater target," *The journal of the acoustical society of America*, vol. 142, no. 2, pp. 653–665, 2017.
- [33] B. Wang, W. Zhang, Y. Zhu, C. Wu, and S. Zhang, "An underwater acoustic target recognition method based on amnet," *IEEE Geoscience and Remote Sensing Letters*, vol. 20, pp. 1–5, 2023.
- [34] J. Gildenblat and contributors, "Pytorch library for cam methods," <https://github.com/jacobgil/pytorch-grad-cam>, 2021.
- [35] W. Jia, M. Sun, J. Lian, and S. Hou, "Feature dimensionality reduction: a review," *Complex & Intelligent Systems*, vol. 8, no. 3, pp. 2663–2693, 2022.
- [36] J. Peeples, D. Suen, A. Zare, and J. Keller, "Possibilistic fuzzy local information c-means with automated feature selection for seafloor segmentation," in *Detection and Sensing of Mines, Explosive Objects, and Obscured Targets XXIII*, vol. 10628. SPIE, 2018, pp. 395–408.
- [37] A. Bommert, X. Sun, B. Bischl, J. Rahnenführer, and M. Lang, "Benchmark for filter methods for feature selection in high-dimensional classification data," *Computational Statistics & Data Analysis*, vol. 143, p. 106839, 2020.